CrossMark

Obliquity Tides May Drive WASP-12b's Rapid Orbital Decay

Sarah Millholland[1] and Gregory Laughlin
Department of Astronomy, Yale University, New Haven, CT 06511, USA; sarah.millholland@yale.edu

Abstract

Recent analyses have revealed a mystery. The orbital period of the highly inflated hot Jupiter, WASP-12b, is decreasing rapidly. The rate of inspiral, however, is too fast to be explained by either eccentricity tides or equilibrium stellar tides. While dynamical stellar tides are possible, they require a subgiant structure for the star, whereas stellar models point toward a main-sequence host. Here, we show that these hitherto irreconcilable observations might be explained by planetary obliquity tides if planet b's spin vector is trapped in a high-obliquity state maintained by a secular spin–orbit resonance with an unseen exterior perturbing planet. We derive constraints on the obliquity ($\epsilon \gtrsim 50°$), reduced tidal quality factor ($Q' \sim 10^6 - 10^7$), and perturbing planet parameters ($M_2 \sim 10 - 20 M_\oplus$, $a_2 \lesssim 0.04$ au) required to generate the observed orbital decay. Direct N-body simulations that include tidal and spin dynamics reinforce the plausibility of the scenario. Furthermore, we show that the resonance could have been captured when planet b's obliquity was small, making the proposed sequence of events easy to explain. The hypothetical perturbing planet is within the limits of current radial velocity constraints on the system, yet it is also detectable. If it exists, it could provide evidence in favor of the in situ formation hypothesis for hot Jupiters.

Key words: planet–star interactions – planets and satellites: detection – planets and satellites: dynamical evolution and stability – planets and satellites: individual (WASP-12b)

1. Introduction

With their ponderous masses, torrid orbits, and swollen radii, hot Jupiters are prone to the influence of tidal forces (Rasio et al. 1996; Ogilvie & Lin 2004). The slow action of tides delineates the structural and dissipative properties of these alien worlds and also points back to their origins. (See Ogilvie 2014 for a review.) To date, however, WASP-12b is the only hot Jupiter whose tidal evolution can be observed in real time. This extremely inflated ($R_p \approx 1.9 R_{\rm Jup}$, $M_p \approx 1.4 M_{\rm Jup}$) gas giant was discovered by Hebb et al. (2009) orbiting a late-F main-sequence star. Maciejewski et al. (2016) and Patra et al. (2017) measured the planet's 1.0914 day transit period to be decreasing on a rapid $P/\dot{P} = -3.2$ Myr timescale.

Apsidal precession could explain the period decrease if the planet's eccentricity is maintained by dynamical perturbations. Maciejewski et al. (2016) and Patra et al. (2017), however, found that this scenario is unlikely, and Bailey & Goodman (2019) showed that it is incompatible with the observations. The planet is spiraling inward. For a plausible stellar tidal quality factor, the rate of decay is roughly three orders of magnitude too large to be explained by equilibrium stellar tides (Bailey & Goodman 2019). Weinberg et al. (2017) showed that dynamical tides can produce a correct decay timescale if the star has evolved off the main sequence. However, recent stellar models by Bailey & Goodman (2019) favor a main-sequence star rather than a subgiant.

WASP-12b's orbital decay thus presents a puzzle. We propose that obliquity tides may provide the solution. When a planet has a nonzero angle between its orbital and spin axes ("obliquity"), tides raised in the planet by the host star produce extremely efficient dissipation (e.g., Levrard et al. 2007). A large obliquity can only be maintained in the face of such dissipation if there is an additional torque, for example, from

the oblate host star or a third body. In these cases, a spin–orbit resonance can develop in which the orbital precession is equal to the planet's spin-axis precession. In an upcoming paper, we show that obliquity-driven dissipation may be a key process in sculpting the observed period distribution of the multiple-transiting planetary systems.

Winn & Holman (2005) suggested that the heat source required to explain the inflated radii of hot Jupiters may, in some cases, be caused by obliquity tides. Levrard et al. (2007), Fabrycky et al. (2007), and Peale (2008) later showed this is unworkable if stellar oblateness is the sole driver of orbital precession. The Winn–Holman scenario requires a nearly 90° obliquity, and the torque induced by the stellar oblateness is too weak to overcome the dissipative tidal torque that acts to damp the obliquity. That is, all isolated hot Jupiters should have zero obliquities. Fabrycky et al. (2007) investigated whether an exterior perturbing planet could drive the requisite orbital precession. They showed that this is unlikely to induce a high-obliquity state for HD 209458b, but the mechanism has not been thoroughly studied for a generalized hot-Jupiter system. Though somewhat fine-tuned, here we show that it can operate in the WASP-12 system, potentially generating the observed orbital decay and implying the existence of a readily detectable companion planet. Figure 1 displays a schematic of the proposed setup.

Constraints on WASP-12b's obliquity and tidal quality factor are discussed in Section 2. Section 3 explores the plausible parameters of the perturbing planet. Using these results, Section 4 presents an N-body simulation in which WASP-12b dissipates due to obliquity tides at a rate matching the observations. Implications and further constraints are discussed in Section 5.

Throughout this work, we adopt the following system parameters. From Maciejewski et al. (2013), we take $P = 1.09142$ days, $R_\star = 1.63 R_\odot$, $\rho_\star = 0.315 \rho_\odot$ (which yields $M_\star = 1.36 M_\odot$), $i = 83°$, and $R_p = 1.89 R_{\rm Jup}$. Using the
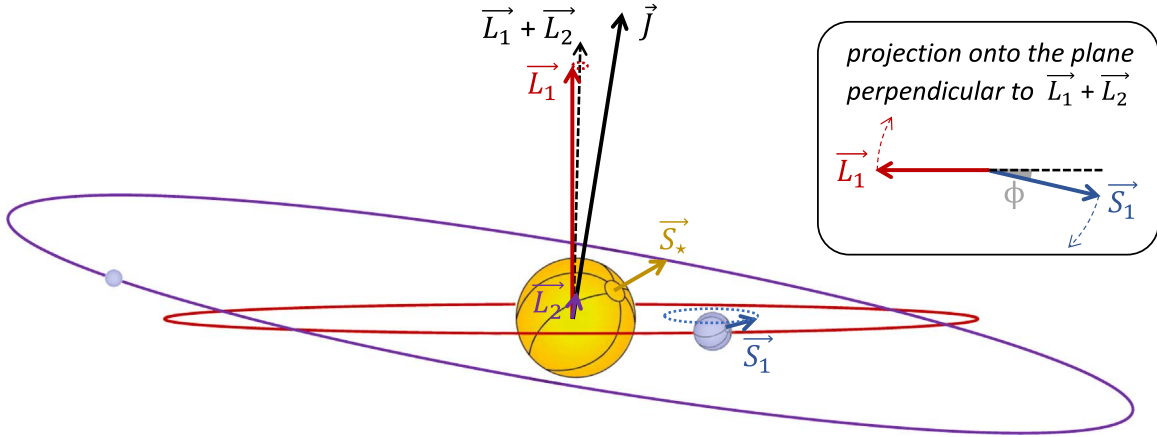

Figure 1. Schematic representation of our proposed scenario. Planet b's obliquity maintains a large value as it is forced by a spin–orbit resonance with an exterior, small-mass planet. The angular momentum vectors are drawn roughly to scale, with the exception of S_1. On short timescales, the orbital angular momentum vector, L_1, precesses about $L_1 + L_2$. The spin angular momentum, S_1, precesses at the same rate, but with a constant phase shift resulting from the tidal dissipation in planet b's interior. (See upper right inset.) On longer timescales, L_1 and $S_\star$ precess around the total vector, J.

$K = 226\,\mathrm{m\,s^{-1}}$ radial velocity semiamplitude obtained by Hebb et al. (2009), the planet mass is $M_p = 1.41 M_{\mathrm{Jup}}$ and $a = 0.02299$ au. We take the rotation period of the star to be $P_\star = 36$ days (Watson & Marsh 2010). Finally, we use the observed period evolution, $P/\dot{P} = -3.2$ Myr, from Patra et al. (2017), so that $a/\dot{a} = -4.8$ Myr.

2. Obliquity Tides

Tidal torques act to synchronize a planet's spin, ω_p, and dampen its eccentricity and obliquity, ϵ_p, to zero, such that energy dissipation ceases. Dissipation can continue, however, if nonzero eccentricities or obliquities are maintained by an external driver. The rate at which orbital energy is converted to heat via tides is a strongly increasing function of obliquity.

We begin by calculating the obliquity and tidal quality factor necessary to explain WASP-12b's observed rate of orbital decay. We assume that $e \approx 0$ (Campo et al. 2011; Croll et al. 2011; Husnoo et al. 2011) and that the spin rate of planet "b" is at equilibrium. Using traditional equilibrium tide theory in the viscous approximation (Hut 1981; Eggleton et al. 1998), as we will throughout this paper, this rate is (Levrard et al. 2007)

$$\omega_{p,\mathrm{eq}} = n\frac{2\cos\epsilon_p}{1 + \cos^2\epsilon_p}. \tag{1}$$

In the presence of both planetary and stellar equilibrium tides, the secular evolution of the semimajor axis is (Leconte et al. 2010)

$$\dot{a} = \frac{4a^2}{GM_\star M_p}\left[K_p\left(\frac{\cos^2\epsilon_p - 1}{\cos^2\epsilon_p + 1}\right) + K_\star\left(\frac{P\cos\epsilon_\star - P_\star}{P_\star}\right)\right]. \tag{2}$$

K_p is given by

$$K_p = \frac{9}{4Q_p'}\left(\frac{GM_\star^2}{R_p}\right)\left(\frac{R_p}{a}\right)^6 n, \tag{3}$$

where $Q_p' = 3Q_p/2k_{2,p}$ is the reduced annual tidal quality factor, with $k_{2,p}$ being the Love number. R_p is the planetary radius, a is the semimajor axis, and $n = 2\pi/P$ is the mean motion. $K_\star$ is defined as in Equation (3) with p and $\star$ subscripts reversed.

If ϵ_p is large, the terms in parentheses multiplying K_p and $K_\star$ are both of order unity. We therefore compare the relative strengths of planetary and stellar tides by taking the ratio,

$$\frac{K_p}{K_\star} = \frac{Q_\star'}{Q_p'}\left(\frac{M_\star}{M_p}\right)^2\left(\frac{R_p}{R_\star}\right)^5. \tag{4}$$

For plausible tidal quality factors, $Q_\star' = 10^8$ (Collier Cameron & Jardine 2018; Penev et al. 2018) and $Q_p' \sim 10^7$ (Bonomo et al. 2017), the ratio is $K_p/K_\star \sim 500$. Bailey & Goodman (2019) found $a/\dot{a} \approx -1.8$ Gyr for equilibrium stellar tides alone. The $\sim$2–3 orders of magnitude increase from obliquity tides is therefore sufficient to reach the observed rate of orbital evolution, $a/\dot{a} = -4.8$ Myr.

Ignoring the $K_\star$ term in Equation (2) and solving for the unknowns, Q_p' and ϵ_p, yields

$$Q_p'\left(\frac{\cos^2\epsilon_p + 1}{\cos^2\epsilon_p - 1}\right) = \frac{9a^{-11/2}}{\dot{a}}\sqrt{GM_\star}\frac{M_\star}{M_p}R_p^5. \tag{5}$$

All quantities on the right-hand side are well-determined observationally. With the parameter values outlined in the introduction, Equation (5) becomes

$$Q_p'\left(\frac{\cos^2\epsilon_p + 1}{\cos^2\epsilon_p - 1}\right) = -8.59 \times 10^6. \tag{6}$$

Figure 2 shows the resulting mutual constraints on ϵ_p and Q_p'. Obliquities, $\epsilon_p \gtrsim 30°$, are consistent with $Q_p' \sim 10^6 - 10^7$. The entirely independent match between the narrow range of values of Q_p' required for the obliquity tide mechanism to work and the a priori expectation for Q_p' is an encouraging sign. In the absence of support, however, tidal torques would damp ϵ_p to zero in a mere 10^4 years. Large obliquities can be sustained if the planet is locked in a secular spin–orbit resonance that is maintained by another applied torque.

3. Secular Spin–Orbit Resonance with an Exterior Perturber

In the constant-obliquity configuration, called a "Cassini state" (Colombo 1966; Peale 1969; Ward 1975), the planet's spin and orbital axes precess at the same rate about the same
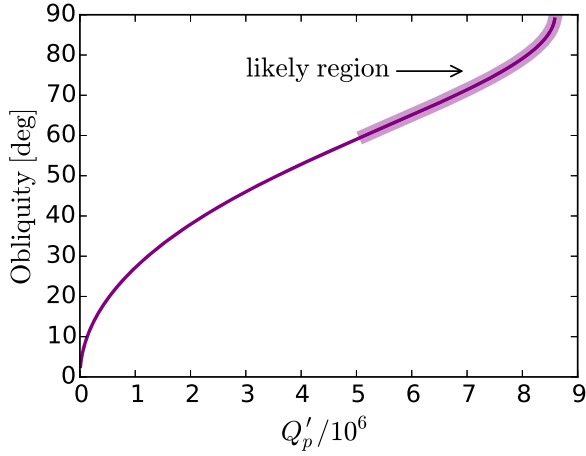
Figure 2. Constraints on the obliquity of planet "b" and $Q'_p = 3Q_p/2k_{2,p}$ in order for agreement with the observed rate of orbital decay. The highlighted region is most likely based on the large expected obliquity (see Section 3).

axis, and they are coplanar in the limit of vanishing dissipation.[2] We argue that the required orbital precession can arise from secular interactions with an additional planet. If this hypothesis is correct, it places strong constraints on the characteristics of the as-yet undetected perturber.

The torque from the host star on a rotationally flattened planet will cause the spin-axis to process about the orbit normal at a period, $T_\alpha = 2\pi/(\alpha \cos \epsilon_p)$, where α is the precession constant. In the absence of satellites, α is given by (Ward & Hamilton 2004; Ragozzine & Wolf 2009)

$$\alpha = \frac{1}{2} \frac{M_\star}{M_p} \left(\frac{R_p}{a} \right)^3 \frac{k_{2,p}}{C_p} \omega_p. \tag{7}$$

C_p is the planet's moment of inertia normalized by $M_p R_p^2$.

The spin-axis precession frequency must be commensurable with the nodal recession frequency, $g = \dot{\Omega}$. In the case that this nodal recession is due to secular perturbations with an exterior planet, the frequency is given by Laplace–Lagrange theory for planets not near mean-motion resonance (Murray & Dermott 1999). To first order in masses and second order in eccentricities and inclinations,[3]

$$g = -\frac{1}{4} b_{3/2}^{(1)}(\alpha_{12}) \alpha_{12} \left(n_1 \frac{M_{p2}}{M_\star + M_{p1}} \alpha_{12} + n_2 \frac{M_{p1}}{M_\star + M_{p2}} \right). \tag{8}$$

Here, $\alpha_{12} = a_1/a_2$ and n_i is the mean motion of planet i. We use the subscripts 1 and 2 to refer to planet b and hypothetical planet c, respectively. The constant, $b_{3/2}^{(1)}(\alpha_{12})$, is a Laplace coefficient, defined by

$$b_{3/2}^{(1)}(\alpha_{12}) = \frac{1}{\pi} \int_0^{2\pi} \frac{\cos \psi}{(1 - 2\alpha_{12} \cos \psi + \alpha_{12}^2)^{3/2}} d\psi. \tag{9}$$

Cassini states obey the resonance condition

$$g \sin(\epsilon_p - I) + \alpha \cos \epsilon_p \sin \epsilon_p = 0, \tag{10}$$

---

[2] There are four Cassini states, but only two of them (states 1 and 2) are stable against tidal dissipation. We refer to Cassini state 2, which is most favorable for maintaining a large obliquity (Fabrycky et al. 2007).
[3] Although the system may not have a small mutual inclination, this expansion is sufficient for a plausibility argument.
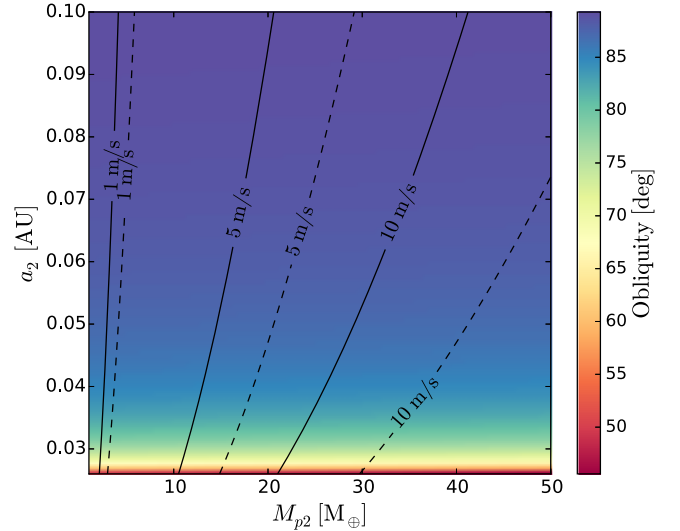

Figure 3. Map of the obliquity that WASP-12b would have if it was captured in spin–orbit resonance with a planet of mass, M_{p2}, and semimajor axis, a_2. The solid/dashed lines are contours of the perturber's RV semiamplitude for $i_2 = 90°/i_2 = 45°$, respectively.

where I is the inclination of the planet's orbital plane with respect to the invariable plane. If the obliquity is large and the perturbing planet is small, then $I \ll \epsilon_p$ and

$$|g| \approx \alpha \cos \epsilon_p. \tag{11}$$

This condition can be applied to calculate the parameter space in the perturber's mass, M_{p2}, and semimajor axis, a_2, that allows for commensurability. When WASP-12b is spinning at its equilibrium rate, Equation (11) becomes

$$|g| = \alpha_{\text{syn}} \frac{2 \cos^2 \epsilon_p}{1 + \cos^2 \epsilon_p}, \tag{12}$$

where $\alpha_{\text{syn}} = \alpha(n/\omega_p)$ is the value of α in the case of synchronous rotation ($\omega_p = n$). The solution for ϵ_p is

$$\cos \epsilon_p = \left(\frac{1}{2\alpha_{\text{syn}}/|g| - 1} \right)^{1/2}. \tag{13}$$

In Figure 3, we show the obliquity necessary for the resonance to hold as a function of M_{p2} and a_2. In addition to the parameters outlined in the introduction, we also adopted $k_{2,p} = 0.1$ and $C_p = 0.2$. The results have little sensitivity to these choices. It is interesting to note that the obliquity is nearly independent of M_{p2}. This is because the limit $M_{p2} \ll M_{p1}$ makes g only very weakly dependent on M_{p2}.

Overlaid on Figure 3 are contours of the exterior planet's radial velocity (RV) semiamplitude. After subtracting the planet b signal, the standard deviation of the residuals of the published RVs (Hebb et al. 2009; Husnoo et al. 2011; Knutson et al. 2014; Bonomo et al. 2017) is $\sim$16 m s^{-1}. The RV semiamplitude of the hypothetical planet must be less than this.

3.1. Secular Orbital Evolution of Planet b

The secular decrease in planet b's semimajor axis induced by tides causes α to increase and $|g|$ to decrease. As a result, the obliquity must increase adiabatically in order to maintain the resonance (Equation (11)). This in turn increases the rate
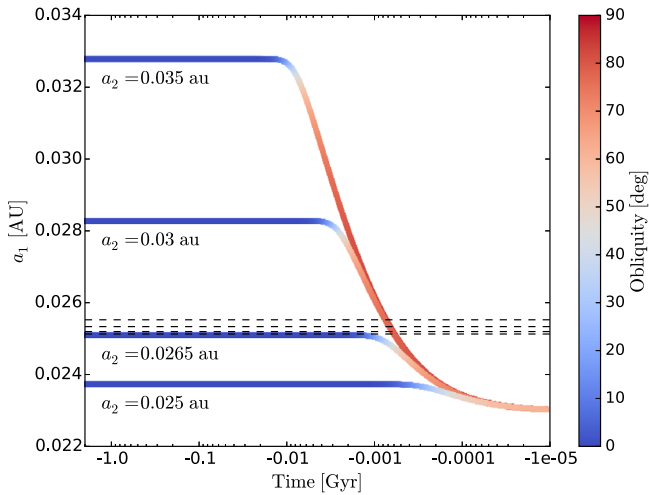
Figure 4. Backward-in-time tidal evolution curves for a_1 corresponding to four different a_2. Planet b's obliquity is assumed to evolve adiabatically according to maintenance of the spin–orbit resonance (Equation (13)). The four horizontal lines show, for each value of a_2, the maximum initial values of a_1 assuming that angular momentum conservation is preserved by damping mutual inclination.

Figure 5. The evolution of planet b's obliquity (gray) and semimajor axis (purple) in the example simulation. The jumps near ~ 0.075 Myr and ~ 0.24 Myr are due to encounters with the 7:3 and 5:2 mean-motion resonances resulting from the divergent tidal migration.

of tidal dissipation. Orbital decay due to obliquity tides is therefore a runaway process.

Here we examine the timescale of this runaway and estimate planet b's past semimajor axis evolution. We do this semianalytically by coupling the secular solution for $\dot{a}_1$ (Equation (2)) with the resonant solution for the obliquity (Equation (13)) in an ODE solver. M_{p2} and a_2 provide the only sensitive dependencies for $a_1(t)$. It also depends on the unknowns $k_{2,p}$ and C_p, which we fix to the fiducial values noted above.

Figure 4 shows four evolutionary trajectories for a_1. They all use $M_{p2} = 20\,M_\oplus$ but have different values of a_2. The initial obliquities were set to the resonant values given by Equation (13), and Q'_p was calculated via Equation (6) so as to recover the observed present-day value of $\dot{a}_1$. The system must conserve total angular momentum as planet b inspirals, which can be accomplished through alignment of L_1 with L_2 and/or $S_\star$ (Fabrycky et al. 2007). If alignment only occurs between L_1 and L_2, we calculate the maximum initial value of a_1 by assuming the mutual inclination, Δi, is currently small but was initially near $90°$ (Batygin et al. 2016). We note that the increase in Δi will slightly modify Equation (8) for g and the timescale at which $a_1(t)$ evolves.

There are several features of interest in Figure 4. First, if angular momentum conservation is preserved solely by aligning L_1 and L_2 (and not $S_\star$), there are strict constraints on the initial value of a_1. Implications of this are discussed in Section 5. Second, it is possible that the obliquity reaches $\epsilon_p \lesssim 1°$ within a billion years into the past of the system's 1.7 ± 0.8 Gyr life (Chan et al. 2011). This is important because it implies that the resonance could have been captured when $\epsilon_p \lesssim 1°$, yet ϵ_p still reached large values by the present day. This makes it unnecessary to invoke an unrealistic large primordial obliquity that might have made the initial resonant capture difficult to explain.

4. Example Simulation

Our investigation thus far has established the plausibility that obliquity tides may be acting on WASP-12b. The analysis,
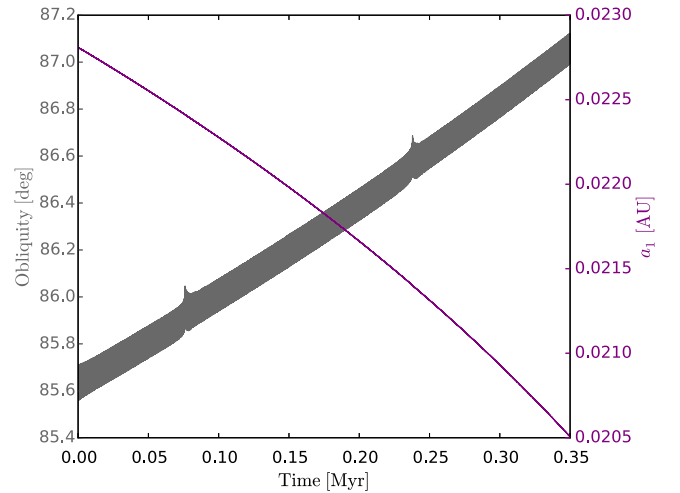
however, has so far only been analytic. Numerical simulations can substantiate the hypothesis by confirming the configuration's stability. Here we present an example simulation that is consistent with all constraints outlined above. We adopt the following parameters for the perturbing planet: $a_2 = 0.04$ au, $M_{p2} = 20\,M_\oplus$, $R_{p2} = 5\,R_\oplus$, $k_{2,p2} = 0.3$, $C_{p2} = 0.25$, and $|i_1 - i_2| = 20°$. We use Equations (5) and (13) to determine the value of planet b's Q_p that agrees with a resonant solution and the observed orbital decay.

We model the tidal, spin, and orbital evolution of the WASP-12 system consisting of the host star, planet b, and the additional planet. Our code consists of direct numerical integrations using instantaneous accelerations in the framework of Mardling & Lin (2002). In addition to the standard Newtonian gravitational accelerations, we also apply accelerations on the planets due to (1) the quadrupolar gravitational moment of the star and (2) equilibrium tides raised in the planets from the star (Hut 1981; Eggleton et al. 1998). We evolve the orbital and spin equations in hierarchical (Jacobi) coordinates using a Bulirsch–Stoer integrator (Press et al. 1992) with the timestep equal to $0.01P_1$ and the timestep accuracy parameter set to $\eta = 10^{-13}$.

A simulation of the present-day system is indifferent to when and how the Cassini state was originally captured. Figure 4 shows that this capture is straightforward to explain because it could have occurred with $\epsilon_p \lesssim 1°$. The capture process requires that $T_\alpha = 2\pi/(\alpha \cos \epsilon_p)$ and $T_g = 2\pi/|g|$ evolve such that T_α/T_g crosses through unity from above. There are many potential scenarios for this (e.g., a decrease in T_α due to tidal synchronization of planet b's spin). Here we solely wish to verify that a scenario consistent with the constraints is capable of existing today, so we use a contrived mechanism to induce the capture. We start with $\epsilon_p = 88°$ and Q_p 10 times larger than the target value. The obliquity damps due to the tidal torque, and T_α/T_g slowly crosses unity from above. After the resonant locking, we decrease Q_p on a 10,000 year exponential timescale until it reaches the target value.

Figure 5 shows the time evolution of planet b's obliquity and semimajor axis during a period well after the capture has taken place and Q_p has been reduced to the target value. At the beginning of the simulation, the semimajor axis is evolving at a

rate, $\dot{a}_1 \approx -0.0048$ au/Myr, in agreement with current observations. $|\dot{a}_1|$ increases as time advances, and ϵ_p increases adiabatically so as to maintain the resonance.

For a dissipative Cassini state, there exists an upper limit at which the tidal torque is as strong as the perturbation torque (here due to the additional planet); beyond that, the resonance can no longer be maintained (Fabrycky et al. 2007; Peale 2008). In our example simulation, the spin vector is phase shifted by $\phi = 13°$ out of the plane defined by $\boldsymbol{L}_1$ and $\boldsymbol{J}$. Fabrycky et al. (2007) showed that the dissipative limit is at $\phi = 90°$, so $13°$ is well away from this. Although the phase shift increases as a_1 decreases and the Cassini state will eventually break, the simulation indicates that the present-day WASP-12 system can most certainly exist within the dissipative limit.

5. Discussion

WASP-12b has been the subject of intense investigation since its discovery in 2009. The obliquity tide hypothesis that we have put forth to explain the planet's rapid orbital decay can resolve additional mysteries. The planet's thermal phase curve presents unusual features (Cowan et al. 2012; Adams & Laughlin 2018) that might be naturally explained using a nonzero obliquity model (A. D. Adams et al. 2018, in preparation). Second, despite its scorching temperature ($T_{eq} \approx 2500$ K), the planet's extreme radius inflation is considered an outlier that cannot be explained without an extra heating mechanism (Miller et al. 2009; Fortney et al. 2011; Ibgui et al. 2011). Obliquity tides can readily provide the heat. If we assume that the energy from orbital decay is radiating from the planet, the energy involved is

$$\frac{dE}{dt} = \frac{(GM_\star)^{3/2}M_p}{6\pi}a^{-5/2}\dot{P} \simeq 5 \times 10^{30} \text{ erg s}^{-1}, \quad (14)$$

implying a tidal luminosity that is of the same order as the insolation received by the planet.

Extreme tidal heating is consistent with the observation that WASP-12b is overflowing its Roche lobe (Haswell et al. 2012) and losing mass at an impressive rate of $\sim 1.6 \, M_\oplus$/Myr (Jackson et al. 2017). These independent signs that the planet is undergoing an end-of-life thermal runaway are compatible with the obliquity tide hypothesis.

To explain the peculiarities of WASP-12, we have invoked a peculiar configuration: a hot Jupiter with an inclined, small planetary companion on a close-in orbit. We investigated the alternative that the requisite orbital precession could be supplied by the torque from stellar oblateness rather than a companion planet (Fabrycky et al. 2007). However, this results in $|g|$ so small that ϵ_p is nearly $90°$, and dissipative torque balance is impossible. Moreover, in this scenario, ϵ_p would decrease as the orbit decays, and this is inconsistent.

While no such difficult-to-detect (Millholland et al. 2016; Millholland & Laughlin 2017), misaligned system is currently known to exist, they are the primary prediction of Batygin et al.'s (2016) theory of in situ formation of hot Jupiters (see also Spalding & Batygin 2017). Confirmation of our obliquity tide hypothesis would make WASP-12 the second system definitively known to host both a hot Jupiter and a nearby companion (Becker et al. 2015) and would provide evidence in support of Batygin et al.'s (2016) prediction.

Further investigations may strengthen or weaken the obliquity tide hypothesis. First, as noted in Section 3.1, the system must conserve angular momentum and if this is solely

via realignment of $\boldsymbol{L}_1$ and $\boldsymbol{L}_2$, then $a_2 \lesssim 0.027$ au is preferred. Though this renders the obliquity tide hypothesis uncomfortably fine-tuned, the rarity of planet b's observed orbital decay favors a short lifetime of the configuration and therefore a small a_2. There is, however, a significant storage of misaligned ($\lambda = 59^{+15}_{-20}°$; Albrecht et al. 2012) angular momentum in $\boldsymbol{S}_\star$. If there is a mechanism for aligning $\boldsymbol{L}_1$ and $\boldsymbol{S}_\star$, the constraints are much less stringent; the limit on the initial value of a_1 is ~ 0.043 au using a conservative estimate of $P_\star$.

Another test of the hypothesis arises from Transit Duration Variations (TDVs) of planet b due to its orbital precession (Miralda-Escudé 2002). The precession period is ~ 15 years, and for mutual orbital inclinations, $\Delta i \lesssim 20°$, we calculate that the maximum peak-to-peak TDV amplitude is

$$\Delta T_{dur} \approx 0.184 \min\left(\frac{\Delta i}{1°}\right)\left(\frac{M_{p2}}{10M_\oplus}\right). \quad (15)$$

If $\Delta i \lesssim 15°$, TDVs would not have been detected in the extant photometry, which has ~ 3 minute transit duration uncertainties (Collins et al. 2017). In addition to TDVs, the perturbing planet may also induce transit timing variations (TTVs). Collins et al. (2017) ruled out *sinusoidal* TTVs with amplitude $\gtrsim 35$ s. If the perturbing planet is nonresonant, the TTVs would certainly be smaller than this. Future photometric monitoring (e.g., by *TESS*) will test our hypothesis by placing tighter constraints on TTVs/TDVs.

RV follow-up is likely the best avenue for falsification of our hypothesis. The RV semiamplitude of the perturbing planet in our example simulation was $K \sim 7 \text{ m s}^{-1}$, and planets with $K \lesssim 10 \text{ m s}^{-1}$ would not yet have been detected in the current data set. This makes WASP-12 an excellent candidate for future high-precision RV surveys.

ORCID iDs

Sarah Millholland ⦿ https://orcid.org/0000-0003-3130-2282
Gregory Laughlin ⦿ https://orcid.org/0000-0002-3253-2621

References

Adams, A. D., & Laughlin, G. 2018, AJ, 156, 28
Albrecht, S., Winn, J. N., Johnson, J. A., et al. 2012, ApJ, 757, 18
Bailey, A., & Goodman, J. 2019, MNRAS, 482, 1872
Batygin, K., Bodenheimer, P. H., & Laughlin, G. P. 2016, ApJ, 829, 114
Becker, J. C., Vanderburg, A., Adams, F. C., Rappaport, S. A., & Schwengeler, H. M. 2015, ApJL, 812, L18
Bonomo, A. S., Desidera, S., Benatti, S., et al. 2017, A&A, 602, A107
Campo, C. J., Harrington, J., Hardy, R. A., et al. 2011, ApJ, 727, 125
Chan, T., Ingemyr, M., Winn, J. N., et al. 2011, AJ, 141, 179
Collier Cameron, A., & Jardine, M. 2018, MNRAS, 476, 2542
Collins, K. A., Kielkopf, J. F., & Stassun, K. G. 2017, AJ, 153, 78
Colombo, G. 1966, AJ, 71, 891
Cowan, N. B., Machalek, P., Croll, B., et al. 2012, ApJ, 747, 82
Croll, B., Lafreniere, D., Albert, L., et al. 2011, AJ, 141, 30
Eggleton, P. P., Kiseleva, L. G., & Hut, P. 1998, ApJ, 499, 853
Fabrycky, D. C., Johnson, E. T., & Goodman, J. 2007, ApJ, 665, 754
Fortney, J. J., Demory, B. O., Désert, J. M., et al. 2011, ApJS, 197, 9
Haswell, C. A., Fossati, L., Ayres, T., et al. 2012, ApJ, 760, 79
Hebb, L., Collier-Cameron, A., Loeillet, B., et al. 2009, ApJ, 693, 1920

Husnoo, N., Pont, F., Hébrard, G., et al. 2011, MNRAS, 413, 2500
Hut, P. 1981, A&A, 99, 126
Ibgui, L., Spiegel, D. S., & Burrows, A. 2011, ApJ, 727, 75
Jackson, B., Arras, P., Penev, K., Peacock, S., & Marchant, P. 2017, ApJ, 835, 145
Knutson, H. A., Fulton, B. J., Montet, B. T., et al. 2014, ApJ, 785, 126
Leconte, J., Chabrier, G., Baraffe, I., & Levrard, B. 2010, A&A, 516, A64
Levrard, B., Correia, A. C. M., Chabrier, G., et al. 2007, A&A, 462, L5
Maciejewski, G., Dimitrov, D., Fernández, M., et al. 2016, A&A, 588, L6
Maciejewski, G., Dimitrov, D., Seeliger, M., et al. 2013, A&A, 551, A108
Mardling, R. A., & Lin, D. N. C. 2002, ApJ, 573, 829
Miller, N., Fortney, J. J., & Jackson, B. 2009, ApJ, 702, 1413
Millholland, S., & Laughlin, G. 2017, AJ, 154, 83
Millholland, S., Wang, S., & Laughlin, G. 2016, ApJL, 823, L7
Miralda-Escudé, J. 2002, ApJ, 564, 1019
Murray, C., & Dermott, S. 1999, Solar System Dynamics (Cambridge: Cambridge Univ. Press)
Ogilvie, G. I. 2014, ARA&A, 52, 171

Ogilvie, G. I., & Lin, D. N. C. 2004, ApJ, 610, 477
Patra, K. C., Winn, J. N., Holman, M. J., et al. 2017, AJ, 154, 4
Peale, S. J. 1969, AJ, 74, 483
Peale, S. J. 2008, in ASP Conf. Ser. 398, Extreme Solar Systems, ed. D. Fischer et al. (San Francisco, CA: ASP), 281
Penev, K., Bouma, L. G., Winn, J. N., & Hartman, J. D. 2018, AJ, 155, 165
Press, W. H., Teukolsky, S. A., Vetterling, W. T., & Flannery, B. P. 1992, Numerical Recipes in FORTRAN, The Art of Scientific Computing (2nd ed.; Cambridge: Cambridge Univ. Press)
Ragozzine, D., & Wolf, A. S. 2009, ApJ, 698, 1778
Rasio, F. A., Tout, C. A., Lubow, S. H., & Livio, M. 1996, ApJ, 470, 1187
Spalding, C., & Batygin, K. 2017, AJ, 154, 93
Ward, W. R. 1975, AJ, 80, 64
Ward, W. R., & Hamilton, D. P. 2004, AJ, 128, 2501
Watson, C. A., & Marsh, T. R. 2010, MNRAS, 405, 2037
Weinberg, N. N., Sun, M., Arras, P., & Essick, R. 2017, ApJL, 849, L11
Winn, J. N., & Holman, M. J. 2005, ApJL, 628, L159